Applied Physics Letters

Impurity band conduction in Si-doped β-Ga_2O_3 films

Cite as: Appl. Phys. Lett. **118**, 072105 (2021); https://doi.org/10.1063/5.0031481
Submitted: 01 October 2020 . Accepted: 30 January 2021 . Published Online: 18 February 2021

Anil Kumar Rajapitamahuni, Laxman Raju Thoutam, Praneeth Ranga, Sriram Krishnamoorthy, and Bharat Jalan

Applied Physics Letters ARTICLE scitation.org/journal/apl

Impurity band conduction in Si-doped β-Ga_2O_3 films

Cite as: Appl. Phys. Lett. **118**, 072105 (2021); doi: 10.1063/5.0031481
Submitted: 1 October 2020 · Accepted: 30 January 2021 ·
Published Online: 18 February 2021

Anil Kumar Rajapitamahuni,[1,a)] Laxman Raju Thoutam,[1,b)] Praneeth Ranga,[2] Sriram Krishnamoorthy,[2] and Bharat Jalan[1,a)]

AFFILIATIONS

[1]Department of Chemical Engineering and Materials Science, University of Minnesota, Minneapolis, Minnesota 55455, USA
[2]Department of Electrical and Computer Engineering, The University of Utah, Salt Lake City, Utah 84112, USA

Note: This paper is part of the Special Topic on Ultrawide Bandgap Semiconductors.
[a)]**Authors to whom correspondence should be addressed:** rajap016@umn.edu and bjalan@umn.edu
[b)]**Now at:** Department of Electronics and Communications Engineering, SR University, Warangal Urban, Telangana 506371, India.

ABSTRACT

By combining temperature-dependent resistivity and Hall effect measurements, we investigate donor state energy in Si-doped β-Ga_2O_3 films grown using metal-organic vapor phase epitaxy. High-magnetic field (H) Hall effect measurements ($-90\,\text{kOe} \leq H \leq +90\,\text{kOe}$) showed non-linear Hall resistance for $T < 150$ K, revealing two-band conduction. Further analyses revealed carrier freeze out characteristics in both bands yielding donor state energies of ~33.7 and ~45.6 meV. The former is consistent with the donor energy of Si in β-Ga_2O_3, whereas the latter suggests a residual donor state. This study provides critical insight into the impurity band conduction and the defect energy states in β-Ga_2O_3 using high-field magnetotransport measurements.

β-Ga_2O_3 possesses wide bandgap (4.6–4.9 eV),[1] high theoretical electrical breakdown (~8 MV/cm),[2] and high conductivity with reasonably high room-temperature mobility,[3] ~184 $cm^2 V^{-1} s^{-1}$, making it an attractive candidate for high-power device applications including ultraviolet (UV) photodetectors.[4–8] Furthermore, access to low-cost, large-scale (up to 6 in.) native substrates with low threading dislocation density (10^3–10^4 cm^{-2}) offers significant advantages for β-Ga_2O_3 epitaxy.[5] β-Ga_2O_3 has monoclinic symmetry (space group C2/m), with lattice parameters of $a = 12.214$ Å, $b = 3.037\,1$ Å, $c = 5.798\,1$ Å, and $\beta = 103.83°$, and is the only stable polymorph of Ga_2O_3 up to the melting point.[9] Within the structure, Ga^{3+} ions are both tetrahedrally and octahedrally coordinated, while O^{2-} ions are either trigonally or tetrahedrally coordinated.[10] This structural complexity complicates the doping study. For instance, it is conceivable that the local electronic structure can vary significantly depending on the dopant size and the sites that it occupies. Despite this obvious challenge, the thermal, optical, and electrical transport properties of β-Ga_2O_3 have been studied extensively, both experimentally and using first-principles calculations[2–5,9,11–24]

Silicon (Si) is shown to be a shallow n-type donor in β-Ga_2O_3.[5,9] Yet, there remains a large inconsistency in the reported ionization energy of Si. For instance, activation energy of donors in Si-doped β-Ga_2O_3 ranges from 16 to 50 meV.[13,25] The variation in donor activation energies has been attributed to the donor density[25] and to the presence of defects and impurities arising from various growth techniques.[26,27] Relatively deeper donors with activation energies of 80–120 meV have also been reported, the origin of which is attributed to the presence of antisites, interstitials, and/or extrinsic impurities.[3,20,28] Deep level states such as DX centers, which are defect complexes formed between the isolated substitutional donor atom (D) and an unknown lattice defect (X), are also studied in β-Ga_2O_3. Using the electron paramagnetic resonance (EPR) study, Son *et al.* reported the DX center in unintentionally doped β-Ga_2O_3 with activation energies of 44–49 meV for partially activated centers, reducing to 17 meV for fully activated DX centers.[29] However, recent transport measurements refuted the presence of DX centers in doped β-Ga_2O_3 based on the low-field magnetotransport analysis.[25] As the presence of DX centers is determinantal for Ga_2O_3-based heterojunction devices, this certainly raises important questions: why there is such discrepancy in the reports of DX centers in β-Ga_2O_3? Can this be due to the variation in the materials depending on the synthesis conditions? Clearly, further investigations of the growth condition-structure-defect-property relationships would help address these questions.

In an attempt to investigate donor state energies in Si-doped β-Ga_2O_3, we performed detailed temperature-dependent magnetotransport studies of homoepitaxial Si-doped β-Ga_2O_3 films grown via

metal-organic vapor phase epitaxy (MOVPE). Low-magnetic field (H) Hall effect measurements ($-20\,\text{kOe} \leq H \leq +20\,\text{kOe}$) showed single band conduction with an activation energy of ~17 meV. In sharp contrast, high-magnetic field ($-90\,\text{kOe} \leq H \leq +90\,\text{kOe}$) Hall effect measurements revealed two-band conduction with activation energies of ~34 and ~46 meV. We discuss the origin of these energy states in the context of Si donor state energy and a residual donor state, respectively.

Si-doped β-Ga_2O_3 films were grown on (010) Fe-doped semi-insulating β-Ga_2O_3 substrates using an MOVPE reactor (Agnitron Agilis). Triethylgallium (TEGa) and molecular O_2 were used as a source of Ga and oxygen in the presence of Ar as a carrier gas. The substrate temperature was fixed at 810 °C. Si was used as an n-type dopant and was controlled by varying the molar ratio of diluted silane (SiH_4) to TEGa.[16] Ohmic contacts were achieved by sputtering Ti/Au (50 nm/50 nm) stacks using shadow mask followed by a rapid thermal annealing at 470 °C in nitrogen for 90 s. Temperature-dependent electrical measurements were performed in Van der Pauw geometry using a physical property measurement system (PPMS® DynaCool™). Excitation currents of 1–10 μA were used.

Figures 1(a) and 1(b) show temperature-dependent resistivity (ρ) and carrier density, respectively, for a 655 nm Si-doped β-Ga_2O_3/Fe-doped β-Ga_2O_3 (010). The schematic of the sample structure is shown in the inset. It is noted that the Hall measurement in the low-field between ±20 kOe yielded linear behavior. The Hall coefficient (R_H) in Fig. 1(b) is, therefore, extracted from the linear slope of Hall resistance (R_{xy}) vs H, where H was varied between ±20 kOe. Temperature dependence carrier density showed a decrease in carrier density from $7.8 \times 10^{17}\,\text{cm}^{-3}$ at 300 K to $6.74 \times 10^{16}\,\text{cm}^{-3}$ at 65 K followed by an

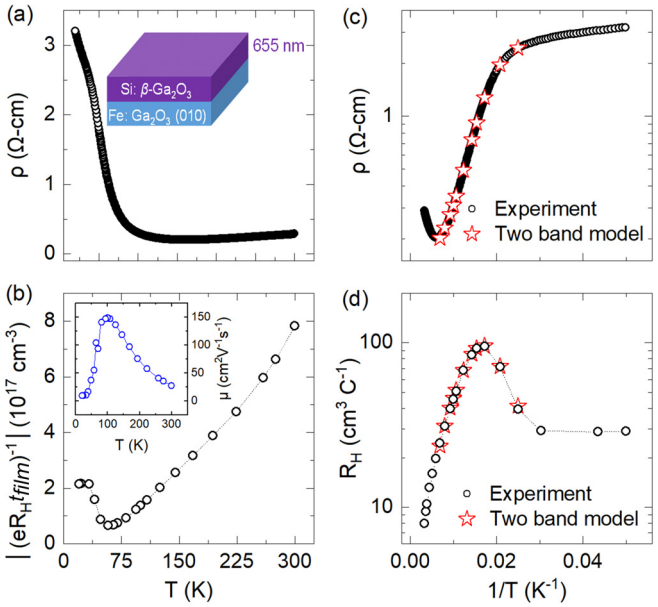

FIG. 1. (a) Temperature-dependent ρ and R_H from a 655 nm Si-doped β-Ga_2O_3/Fe-doped β-Ga_2O_3 (010). The inset shows the schematic of the sample structure. (b) 3D carrier density $(eR_Ht_{film})^{-1}$ as a function of temperature, where R_H is the Hall coefficient, t_{film} is the film thickness, and e is an electronic charge. (c) and (d) Arrhenius plots of ρ and R_H. The red symbols in parts (c) and (d) are calculated ρ and R_H using the two-band conduction model.

unexpected upturn at low temperatures, $40 \leq T \leq 65$ K, which saturates to a value of $2.15 \times 10^{17}\,\text{cm}^{-3}$ for $T < 40$ K. The inset shows electron mobility as a function of temperature, revealing drift-diffusive transport as evident from the relatively high low-temperature mobility of $\sim 10\,\text{cm}^2\text{V}^{-1}\text{s}^{-1}$ for $T < 40$ K. To further elucidate this observation, we show in Figs. 1(c) and 1(d) Arrhenius plots of ρ and R_H, revealing nominally three distinct regimes: (i) $225 \leq T \leq 300$ K where ρ decreases and R_H increases with decreasing temperature, (ii) $65\,\text{K} \leq T \leq 225$ K where there is a rapid increase in ρ with decreasing temperature accompanied by an increase in R_H, and (iii) $40 \leq T \leq 65$ K where ρ continues to increase with decreasing temperature but now R_H begins to decrease. Below 40 K there is nearly no variation in R_H. This behavior is remarkably similar to the previously observed temperature dependence of ρ and R_H in doped germanium (Ge) and other heavily doped semiconductors.[30,31] These characteristics have further been attributed to impurity band conduction where carrier conduction occurs in both conduction and impurity bands. Most recently, Kabilova *et al.* also observed an identical behavior in Sn-doped β-Ga_2O_3 and attributed it to the two-band conduction.[32] At higher T, conduction is dominated by electrons in the conduction band, whereas at low temperatures, donor-derived impurity band conduction dominates.[31] Given two-band conduction and drift-diffusive transport, one can, therefore, write the overall resistivity and Hall coefficient (R_H) as

$$\rho(T) = t_{film}(n_1 e \mu_1 + n_2 e \mu_2)^{-1}, \tag{1}$$

$$R_H = \left(n_1\mu_1^2 + n_2\mu_2^2\right)\left(e\left(n_1\mu_1 + n_2\mu_2\right)^2\right)^{-1}, \tag{2}$$

where (n_1, μ_1) and (n_2, μ_2) represent the temperature-dependent sheet carrier density and mobility in the conduction band and the impurity band, respectively. t_{film} represents the film thickness.

To further investigate two-band conduction in our films, we performed high-field Hall measurements. Figure 2(a) shows R_{xy} as a function of H at $40\,\text{K} \leq T < 150$ K. H was swept between ± 90 kOe. Longitudinal resistance (R_{xx}) as a function of H is shown in supplementary material Fig. S1, revealing a positive magnetoresistance behavior at all temperatures, whereas R_{xy} (H) showed non-linearity as illustrated in Fig. 2(a). The latter is consistent with two-band conduction. It is also noted that the non-linearity arising from the magnetic field dependence of the Hall scattering factor is ruled out (see the supplementary material). We analyzed our experimental results using the two-band conduction model. In this model, R_{xy} (H) can be written as

$$R_{xy}(H) = \frac{-(H/e)\left[\left(n_1\mu_1^2 + n_2\mu_2^2\right) + H^2\mu_1^2\mu_2^2\left(n_1 + n_2\right)\right]}{\left[\left(n_1\mu_1 + n_2\mu_2\right)^2 + H^2\mu_1^2\mu_2^2\left(n_1 + n_2\right)^2\right]}. \tag{3}$$

In this equation, there are four unknowns (n_1, μ_1 n_2, and μ_2) that can be further reduced to two unknowns by calculating Hall conductance, $G_{xy}(H)$ using experimentally measured $R_{xy}(H)$ and $R_{xx}(H)$,

$$G_{xy}(H) = -\frac{R_{xy}}{\left(R_{xy}^2 + R_{xx}^2\right)} = eH\left(\frac{(C_1\mu_1 - C_2)}{\left(\frac{\mu_1}{\mu_2} - 1\right)\left(1 + \mu_2^2H^2\right)} + \frac{(C_1\mu_2 - C_2)}{\left(\frac{\mu_2}{\mu_1} - 1\right)\left(1 + \mu_1^2H^2\right)}\right), \tag{4}$$

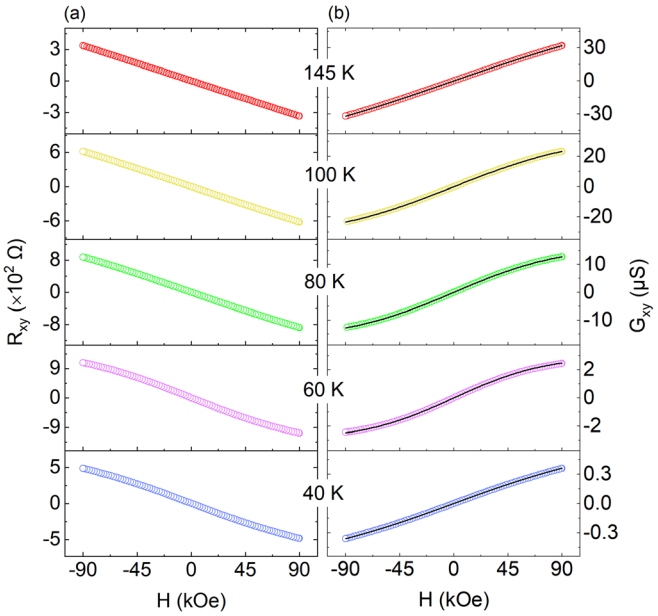

FIG. 2. (a) R_{xy} vs H at $T < 150$ K showing non-linear behavior. (b) Hall conductance, $G_{xy} = -R_{xy}/\left(R_{xy}^2 + R_{xx}^2\right)$, along with fits (black solid lines) using the two-band conduction model.

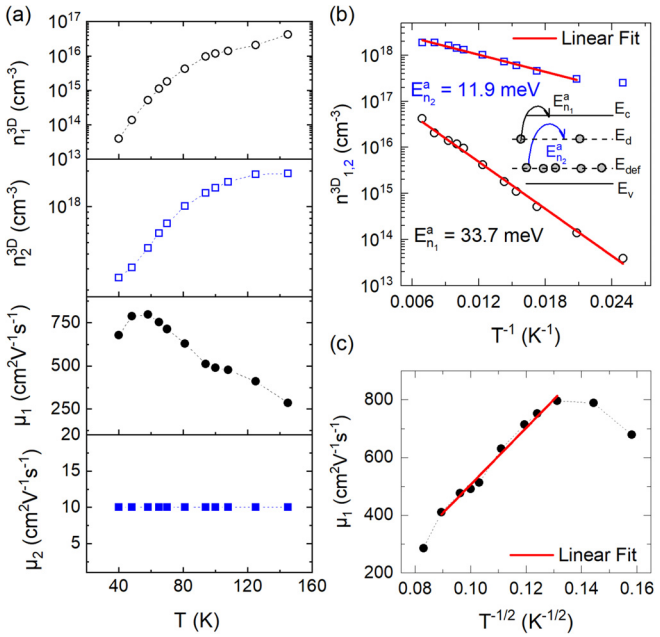

FIG. 3. (a) 3D carrier densities, n_1^{3D} and n_2^{3D}, and their corresponding mobilities μ_1 and μ_2 extracted from the two-band conduction model as a function of temperature. (b) Arrhenius plots with linear fits for n_1^{3D} and n_2^{3D} with corresponding activation energies E^a_{n1} and E^a_{n2}. The inset shows defect state energies illustrating E^a_{n1} and E^a_{n2}. Here, E_d and E_{def} refer to the Si donor state and residual state energies, respectively, within the bandgap. (c) μ_1 vs $T^{-1/2}$ along with a linear fit. The dashed lines are given as guides to the eye.

where $C_1 = n_1\mu_1 + n_2\mu_2$ and $C_2 = n_1\mu_1^2 + n_2\mu_2^2$. It should be noted that C_1 and C_2 are known experimentally from the conductance and the linear slope of the Hall conductance at zero magnetic field, respectively. Details of this analysis can be found elsewhere.[33] Figure 2(b) shows calculated $G_{xy}(H)$ along with fits (solid lines) using Eq. (4) at different temperatures, revealing an excellent match between experiments and the two-band conduction model. This analysis yielded μ_1 and μ_2 (from the fits), which, in turn, allowed us to calculate n_1 and n_2.[33]

Figure 3 shows T-dependent n_1, μ_1, n_2, and μ_2 at $40\ \text{K} \le T \le 150$ K. Using n_1, μ_1 n_2, and μ_2 as a function of T, we calculated ρ and R_H using Eqs. (1) and (2). The calculated ρ (T) and R_H (T) are shown in Figs. 1(c) and 1(d) using open red symbols, revealing an excellent match with experimental data. Our analysis, therefore, shows self-consistent results providing further confidence in the two-band conduction model. We, however, note that our analysis yielded reasonably good fits with similar values of μ_1 and for a μ_2 value between 0.1 and $10\ \text{cm}^2\text{V}^{-1}\text{s}^{-1}$. In Fig. 3(a), we show $\mu_2 = 10\ \text{cm}^2\text{V}^{-1}\text{s}^{-1}$, which is closer to the mobility values at low temperature using our low-field Hall measurements and is also reported for impurity band conduction in β-Ga_2O_3.[13,15,34] It is also noted that this value of $\mu_2 = 10\ \text{cm}^2\text{V}^{-1}\text{s}^{-1}$ remains independent of T for $T < 40$ K as shown in the inset of Fig. 1(b). On the other hand, μ_1 first increases with decreasing temperature, reaching a peak value of $796\ \text{cm}^2\text{V}^{-1}\text{s}^{-1}$ at 65 K, and then begins to decrease. The increase in μ_1 follows $T^{-0.5}$ behavior [Fig. 3(c)], which is consistent with phonon-related scattering in β-Ga_2O_3 in agreement with the previous reports,[14,25] whereas the drop in mobility for $T < 65$ K is consistent with the ionized impurity scattering. Significantly, this temperature is the same at which R_H was found to decrease in Fig. 1(d), suggesting that the scattering centers are likely the donor-derived ionized impurities. Unlike μ_1, μ_2 was found to be low and T-independent, which is again consistent with the presence of the impurity band.[13,15]

We now turn to the discussion of donor state energy. First, we present results from the analyses of low-field Hall effect measurements, yielding single band conduction with an activation energy of ~17 meV (supplementary material Fig. S2). This energy state is in good agreement with the published results of Si activation energy in Si-doped β-Ga_2O_3 near the Mott insulator-to-metal transition.[25] However, our analyses using high-field Hall effect measurements resulted in a deeper understanding of transport activation behavior. Figure 3(b) shows Arrhenius plots for n_1^{3D} (n_1/t_{film}) and n_2^{3D} (n_2/t_{film}) extracted from the two-band conduction model. This plot yielded linear slopes with activation energies of $E_a^{n_1} = 33.7$ meV and $E_a^{n_2} = 11.9$ meV, respectively. The donor ionization energy of Si in β-Ga_2O_3 is reported to be ~36 meV, which is close to $E_a^{n_1}$, suggesting that Si shallow donors are the source of high-mobility carriers and that they are responsible for conduction at higher temperatures.[13,25] The corresponding high mobilities, $285\ \text{cm}^2\text{V}^{-1}\text{s}^{-1}$ ($T = 150$ K) $< \mu_1 <$ $678\ \text{cm}^2\text{V}^{-1}\text{s}^{-1}$ (40 K), further corroborate with the transport occurring in the conduction band. In addition, we found a residual donor state ~12 meV lying below the primary Si donor state, as shown schematically in the inset of Fig. 3(b), with a donor state energy of 45.6 meV (= 33.7 + 11.9 meV). We note that our analyses have assumed the temperature-independent μ_2 as discussed above. Previously, a defect state with an activation energy of 46 meV below conduction band minima has been attributed to the DX center.[29] We,

however, note that while this study provides evidence of a residual donor state at ∼46 meV, it is non-trivial to assign it to a specific defect type. It should also be noted that our analysis does not account for the Hall scattering factor, which can depend on both the temperature and the magnetic field and can, therefore, also influence the carrier density.[14] Future study should be directed to investigate the relationship between synthesis conditions and defect formation in β-Ga_2O_3.

In summary, we have investigated donor state energy in doped β-Ga_2O_3 films via temperature-dependent resistivity and Hall effect measurements. The two-band conduction model described experimental data in addition to yielding donor state energies, ∼34 meV and ∼46 meV, which we attribute to the Si donor and a potential DX center, respectively. In contrast, low-field transport yielded only one carrier type with an activation energy of ∼17 meV in agreement with the published results. Our work provides critical insight into the nature of the donor types in Si-doped β-Ga_2O_3 with implications in the development of high-power electronic devices.

See the supplementary material for magnetoresistance data, the temperature dependence of the low-field measured Hall carrier density, and our discussion on the role of the Hall scattering factor in β-Ga_2O_3.

This work was supported primarily by the National Science Foundation through the University of Minnesota MRSEC under Award No. DMR-2011401. Part of this work was supported through the Air Force Office of Scientific Research (AFOSR) through Grant No. FA9550-19-1-0245 and through No. DMR-1741801. Portions of this work were conducted in the Minnesota Nano Center, which was supported by the National Science Foundation (NSF) through the National Nano Coordinated Infrastructure Network (NNCI) under Award No. ECCS-1542202. Part of this work was also carried out in the College of Science and Engineering Characterization Facility, University of Minnesota, which received capital equipment funding from the NSF through the UMN MRSEC program. Thin film synthesis work at the University of Utah was supported primarily by the Air Force Office of Scientific Research under Award No. FA9550-18-1-0507 monitored by Dr. Ali Sayir. Any opinions, findings, and conclusions or recommendations expressed in this material are those of the authors and do not necessarily reflect the views of the United States Air Force. Material synthesis effort at the University of Utah also acknowledges support from the National Science Foundation (NSF) under Award No. DMR-1931652. Part of this work was performed at the Utah Nanofab sponsored by the College of Engineering and the Office of the Vice President for Research.

DATA AVAILABILITY

The data that support the findings of this study are available from the corresponding author upon reasonable request.

REFERENCES

[1]H. H. Tippins, Phys. Rev. **140**(1A), A316 (1965).
[2]M. Higashiwaki, K. Sasaki, A. Kuramata, T. Masui, and S. Yamakoshi, Appl. Phys. Lett. **100**(1), 013504 (2012).
[3]Z. Feng, A. F. M. Anhar Uddin Bhuiyan, M. R. Karim, and H. Zhao, Appl. Phys. Lett. **114**(25), 250601 (2019).
[4]M. Higashiwaki, K. Sasaki, H. Murakami, Y. Kumagai, A. Koukitu, A. Kuramata, T. Masui, and S. Yamakoshi, Semicond. Sci. Technol. **31**(3), 034001 (2016).
[5]J. Zhang, J. Shi, D.-C. Qi, L. Chen, and K. H. L. Zhang, APL Mater. **8**(2), 020906 (2020).
[6]A. Atilgan, A. Yildiz, U. Harmanci, M. T. Gulluoglu, and K. Salimi, Mater. Today **24**, 101105 (2020).
[7]D. Y. Guo, K. Chen, S. L. Wang, F. M. Wu, A. P. Liu, C. R. Li, P. G. Li, C. K. Tan, and W. H. Tang, Phys. Rev. Appl. **13**, 024051 (2020).
[8]M. I. Pintor-Monroy, B. L. Murillo-Borjas, and M. A. Quevedo-Lopez, ACS Appl. Electron. Mater. **2**, 3358 (2020).
[9]J. Åhman, G. Svensson, and J. Albertsson, Acta Cryst. **C52**, 1336–1338 (1996).
[10]S. Geller, J. Chem. Phys. **33**, 676 (1960).
[11]A. J. Green, K. D. Chabak, E. R. Heller, R. C. Fitch, M. Baldini, A. Fiedler, K. Irmscher, G. Wagner, Z. Galazka, S. E. Tetlak, A. Crespo, K. Leedy, and G. H. Jessen, IEEE Electron Device Lett. **37**(7), 902 (2016).
[12]M. Higashiwaki, K. Sasaki, T. Kamimura, M. H. Wong, D. Krishnamurthy, A. Kuramata, T. Masui, and S. Yamakoshi, Appl. Phys. Lett. **103**(12), 123511 (2013).
[13]K. Irmscher, Z. Galazka, M. Pietsch, R. Uecker, and R. Fornari, J. Appl. Phys. **110**(6), 063720 (2011).
[14]N. Ma, N. Tanen, A. Verma, Z. Guo, T. Luo, H. Xing, and D. Jena, Appl. Phys. Lett. **109**(21), 212101 (2016).
[15]T. Oishi, Y. Koga, K. Harada, and M. Kasu, Appl. Phys. Express **8**(3), 031101 (2015).
[16]P. Ranga, A. Rishinaramangalam, J. Varley, A. Bhattacharyya, D. Feezell, and S. Krishnamoorthy, Appl. Phys. Express **12**(11), 111004 (2019).
[17]K. Sasaki, M. Higashiwaki, A. Kuramata, T. Masui, and S. Yamakoshi, J. Cryst. Growth **392**, 30 (2014).
[18]J. B. Varley, J. R. Weber, A. Janotti, and C. G. Van de Walle, Appl. Phys. Lett. **97**(14), 142106 (2010).
[19]E. G. Víllora, K. Shimamura, T. Ujiie, and K. Aoki, Appl. Phys. Lett. **92**(20), 202120 (2008).
[20]Y. Zhang, F. Alema, A. Mauze, O. S. Koksaldi, R. Miller, A. Osinsky, and J. S. Speck, APL Mater. **7**(2), 022506 (2019).
[21]H. Zhou, K. Maize, G. Qiu, A. Shakouri, and P. D. Ye, Appl. Phys. Lett. **111**(9), 092102 (2017).
[22]F. Orlandi, F. Mezzadri, G. Calestani, F. Boschi, and R. Fornari, Appl. Phys. Express **8**(11), 111101 (2015).
[23]K. Ghosh and U. Singisetti, Int. J. High Speed Electron. Syst. **28**, 1940008 (2019).
[24]Z. Feng, A. F. M. Anhar Uddin Bhuiyan, Z. Xia, W. Moore, Z. Chen, J. F. McGlone, D. R. Daughton, A. R. Arehart, S. A. Ringel, S. Rajan, and H. Zhao, Phys. Status Solidi RRL **14**, 2000145 (2020).
[25]A. T. Neal, S. Mou, S. Rafique, H. Zhao, E. Ahmadi, J. S. Speck, K. T. Stevens, J. D. Blevins, D. B. Thomson, N. Moser, K. D. Chabak, and G. H. Jessen, Appl. Phys. Lett. **113**(6), 062101 (2018).
[26]S. Lany, APL Mater. **6**(4), 046103 (2018).
[27]M. D. McCluskey, J. Appl. Phys. **127**(10), 101101 (2020).
[28]A. T. Neal, S. Mou, R. Lopez, J. V. Li, D. B. Thomson, K. D. Chabak, and G. H. Jessen, Sci. Rep. **7**(1), 13218 (2017).
[29]N. T. Son, K. Goto, K. Nomura, Q. T. Thieu, R. Togashi, H. Murakami, Y. Kumagai, A. Kuramata, M. Higashiwaki, A. Koukitu, S. Yamakoshi, B. Monemar, and E. Janzén, J. Appl. Phys. **120**(23), 235703 (2016).
[30]H. Fritzsche and M. Cuevas, Phys. Rev. **119**(4), 1238 (1960).
[31]N. F. Mott and W. D. Twose, Adv. Phys. **10**(38), 107 (1961).
[32]Z. Kabilova, C. Kurdak, and R. L. Peterson, Semicond. Sci. Technol. **34**, 03LT02 (2019).
[33]N. Bansal, Y. S. Kim, M. Brahlek, E. Edrey, and S. Oh, Phys. Rev. Lett. **109**(11), 116804 (2012).
[34]T. Oishi, K. Harada, Y. Koga, and M. Kasu, Jpn. J. Appl. Phys., Part 1 **55**(3), 030305 (2016).